A DECADE OF PROGRESS IN TOPO-BATHYMETRIC LASER SCANNING EXEMPLIFIED BY THE PIELACH RIVER DATASET

G. Mandlburger[a,*], M. Pfennigbauer[b] , R. Schwarz [b], F. Pöppl [a]

[a] TU Wien, Department of Geodesy and Geoinformation, Austria - gottfried.mandlburger [florian.poeppl]@geo.tuwien.ac.at
[b] RIEGL Laser Measurement Systems GmbH, Austria - mpfennigbauer[rschwarz]@riegl.com

KEY WORDS: Airborne Laser Bathymetry, Integrated sensor orientation, Depth penetration, Exponential decomposition, Full waveform averaging

ABSTRACT:

Topo-bathymetric laser scanning featuring high spatial resolution and a seamless transition within the littoral zone from land to water evolved considerably in the last decade due to progress in both sensor technology and processing methods. Unlike early systems that focused solely on maximizing depth of penetration, topo-bathymetric scanners enable detailed description of coastal and inland waters at a level of detail that opens up applications in hydromorphology, hydraulic engineering, ecohydraulics, and hydrobiology. Since 2013, a near-natural river section of the pre-alpine Pielach River has been repeatedly surveyed with bathymetric LiDAR sensors from manned and unmanned aerial platforms. The captured time series not only constitutes a valuable data basis for analyzing morphometric change in response to recurring flood peaks, but also allows to trace the progress in sensor, platform and data processing technology. In this contribution we demonstrate that over the last ten years, the depth performance could be increased by approximately 60 %, starting from 1 Secchi depths to more than 2 Secchi depths with sub-m spatial resolution. We furthermore focus on current approaches for improving the geometric sensor calibration, which allow integrated processing of GNSS-, IMU- and LiDAR observations for concurrent calculation of both flight trajectories and 3D point clouds with an absolute accuracy better than 5 cm. This is specifically important for repeat surveys and monitoring of fluvial processes. While this contribution confirms substantial progress in the field, further topics like precise modeling of dynamic water surfaces, full waveform processing in complex target situations including littoral vegetation and submerged deadwood, and detection and modeling of underwater vegetation are identified as future research areas.

1. INTRODUCTION

Since the first application of green lasers for coastal mapping (Guenther and Goodman, 1978) around 50 years ago, Airborne Laser Bathymetry (ALB) featured an unbroken progress due to advancements in both sensor and platform technology. In the classic ALB scanner design, infrared (IR) and green laser pulses are emitted simultaneously and co-axially (Guenther et al., 2000). The IR channel delivers returns from the water surface and green laser radiation penetrates the water body and reflects at the water bottom (Philpot, 2019). Concerning depth penetration, the water's optical properties, physically described by effective attenuation k, constraints the achievable penetration depth (Gordon et al., 1975). As an alternative for k, the Secchi depth SD (Effler, 1988) is an empirical measure for water turbidity. System manufacturers often specify the maximum depth performance of a sensor in multiples of the Secchi depth (Quadros, 2013). With careful system design, sensors aiming at maximizing depth penetration achieve around 3 SD while still fulfilling the strict Special Order specification issued by the International Hydrographic Organization (IHO, 2020) requesting a total vertical uncertainty of less than 25 cm (Eren et al., 2019).

Such deep bathymetric sensors are suitable for large water bodies like coastal areas but, due their coarse spatial resolution of 2-5 m, they are not appropriate for capturing small or medium sized inland running waters. For capturing small and morphologically complex rivers, the use of ALB became feasible with the advent of topo-bathymetric laser scanners around 15 years ago (Kinzel et al., 2013). Such sensors utilize short and collimated green laser pulses to measure both objects above, on and below the water surface at high scan rates in the order of 500 kHz. This results in a single strip point density of more than 20 points/m^2, when flown at nominal flying altitudes of around 600 m above ground level (agl) with a speed of approximately 120 knots. Although eye safety is an issue also for this type of instruments, the relatively moderate beam divergence in the order of 1 mrad entails a laser footprint diameter of 50-60 cm, which in turn enables detection of small submerged topographic details like boulders (Hansen et al., 2021).

In the recent years, the development of compact and lightweight bathymetric scanners even allow integration on uncrewed aerial vehicles (UAV). Modern UAV-based bathymetric laser scanners are typically operated from 50-150 m agl. The short measurement distances result in smaller laser footprints, which, together with a high pulse repetition rate, lead to spatial resolution in the dm-range, enabling new fields of application such as grain roughness estimation and object detection (Wang et al., 2022).

From a data processing perspective, major advances have been achieved for (i) georeferencing of Light Detection And Ranging (LiDAR) measurements and (ii) bathymetric full waveform analysis in the recent years, both of which are relevant to ALB. While precise co-registration of the flight strips is a prerequisite for exploiting the full geometric details contained in the point cloud, high absolute accuracy of individually captured flight blocks is required for monitoring applications (hydromorphology, hydraulic engineering, etc.).

Georeferencing is an essential step in ALB data processing to

* Corresponding author

transform the laser ranging measurements from the scanner's coordinate system to a earth-referenced coordinate system. For positioning and orientation, the sensor platform integrates a global satellite navigation system (GNSS) and inertial navigation system (INS). The standard processing pipeline is based on Kalman filtering of GNSS and INS data to obtain a platform trajectory, from which a point cloud may be obtained by direct georeferencing. If the trajectory or the system calibration (boresight, lever arms) is not sufficiently accurate, a subsequent strip adjustment (Glira et al., 2019) may be used to improve the calibration and correct errors in the trajectory. Recently, holistic methods integrating navigation data and imaging sensor data in a single combined trajectory estimation and system calibration have been gaining attraction (Cucci et al., 2017, Brun et al., 2022). In theory, such methods outperform the decoupled processing of navigation data and scan measurements, but have yet to prove themselves in practical mapping situations.

Another crucial step in the ALB processing pipeline is full waveform signal analysis (Xing et al., 2019). While Gaussian decomposition (GDC) is an established approach for topographic laser scanning, volume backscattering in the water column leads to pronounced assymetry of the received pulse waveform with an exponential shape of the falling pulse slope. Analogously to the idea of Gaussian decomposition, one can also represent the system waveform as a superposition of exponential partial pulses whose convolution with the exponential backscatter is again part of the class of exponential sums. This consequently leads to an approach referred to as Exponential Decomposition (XDC) (Schwarz et al., 2017), which was further narrowed down to typical bathymetric target situations where the laser beam interacts with the surface, the volume and the bottom (SVB) (Schwarz et al., 2019). In general, the signal received by a laser sensor operating in linear mode can be described as the convolution of a *system waveform* and the differential backscatter cross section (dBSCS), which is schematically sketched for both topographic and bathymetric target situations in Figure 1.

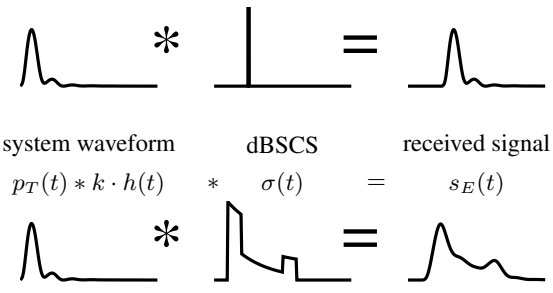

Figure 1. Convolution model. Upper row: discrete scatter case, lower row: distributed scatter case, e. g. surface, volume and bottom contributions of a water column.

Since 2013, an approximately 7 km long section of the prealpine Pielach River near Loosdorf (Lower Austria) serves as a test site (i) for the calibration of new sensors from *RIEGL* Laser Measurement Systems and (ii) for scientific experiments related to topo-bathymetric laser scanning (Mandlburger et al., 2015). The survey area includes the nature reserve *Neubacher Au*, where the river exhibits a meandering course that is subject to hydromorphological changes of the river's gravel bed in response to annual floods and other discharge peaks. The riffle-pool type river has a heterogeneous depth distribution ranging from very shallow ($\leq$50 cm) to around 4 m and a varying shape of the water surface ranging from almost still in deep backwater areas to wavy in shallow riffle sections. Next to the river, a dozen freshwater ponds are located in the surrounding flood plain. These ponds exhibit a depth of up to 5 m, which are hard to penetrate due to a considerable sediment concentration mainly caused by fish stirring up the muddy bottom. All these characteristics make the area an ideal test site for bathymetric laser scanning. With at least one data acquisition per year, the time series represents a valuable data set to track advances in both sensor technology and data processing.

Based on the acquired data at the Pielach River over the last decade, the specific research questions for this paper are: (i) Is it possible to improve state-of-the-art methods for precise alignment and georeferencing of ALB flight strips (Glira et al., 2019) by integrating the measurements from GNSS, INS and LiDAR in a single integrated adjustment? (ii) Is it possible to demonstrate progress in sensor technology by analyzing the evolution of depth penetration over the last ten years when applying the same detection strategy, namely Online Waveform Processing (Pfennigbauer et al., 2014), to the same water body? (iii) Is it possible to further improve the depth penetration performance by applying a new full waveform averaging strategy based on the established approach of exponential decomposition?

The remainder of the article is structured as follows: Section 2 contains a short description of the used sensors and their development over the last ten years. Section 3 introduces the study area and the selected data sets for data processing and evaluation. In Section 4, we describe the employed data processing methods and we discuss the results in Section 5. The article ends with concluding remarks in Section 6.

2. SENSORS AND PLATFORMS

2.1 Employed LiDAR sensors

The evolution of the sensors employed is reflected in the parameters of the survey flights and the resulting 3D point clouds. *RIEGL*'s first airborne laser bathymetry instrument[1], the VQ-820-G was used from helicopters and fixed-wing aircraft at the beginning of the Pielach River campaign in 2013. The VQ-820-G is a single-channel, green-only lidar instrument with an arc-shaped scan pattern, online waveform processing (OWP, cf. section 2.2), and waveform recording for a subset of the measurements. The VQ-820-G's scan mechanism has a field of view (FOV) of 42°, the measurement rate is 200 kHz.

This lidar instrument was followed by the VQ-880-G and later by the VQ-880-G II , which are hybrid ALB systems featuring one green and one IR LiDAR channel, camera(s), and an Inertial Measurement Unit (IMU) mechanically tightly integrated to form a unit that is comparatively easy to mobilize. The green channel performs a circular scan while the IR channel's scan pattern is a slightly-bent, basically nadir-looking arc, both covering a cross-track FOV of 40°. Compared to its predecessor, the VQ-880-G II features a higher measurement rate for the green channel of up to 700 kHz and an improved performance of the IR channel with respect to both measurement rate and ranging capabilities. Weighing approximately 65 kg, the VQ-880-G-series systems are intended for fixed-wing aircraft or crewed helicopter operations.

In 2018, a comparatively small, single-channel ALB system with integrated camera, IMU and data storage was released with

[1] http://www.riegl.com/nc/products/airborne-scanning/

VQ-820-G VQ-880-G VQ-880-G II VQ-840-G

Figure 2. Sensors employed for data acquisition at the Pielach River between 2013 and 2023.

parameter	VQ-820-G	VQ-880-G	VQ-880-G II	VQ-840-G
effective measurement rate [kHz]	200	550	700	200
depth performance [Secchi depths]	1	1.5	1.5	2
nominal flying altitude [m]	600	600	600	150
mass [kg]	26	65	65	14
scan pattern, off-nadir angle	arc, 42°	circle, 40°	circle, 40°	elliptic, ±20°/±14°

Table 1. Sensor parameters

a total weight of less than 15 kg. The scan pattern is nearly elliptical with ±20° FOV cross-track and ±14° FOV along track, the measurement rate is up to 200 kHz. Table 1 summarizes the key parameters of all employed instruments. Images of the sensors are displayed in Figure 2.

2.2 Full waveform recording and online waveform processing

All sensors used in this study can record full waveform data for further analysis in post-processing. The effective rate at which sampled waveform blocks are stored, the length of the sample blocks, and the way their locations within the range gate is determined generally depend on the instrument type and the chosen measurement rate. Waveform recording can be triggered by signal detection performed on the digitized echo signal within the instrument in real-time. This *conditional* waveform storage has the advantage that little excess data is written to the storage device, as the target detection acts as a filter to record only potentially "interesting" parts of the return signal. The downside, however, is that signals slightly below the detection threshold are not available for sophisticated waveform analysis methods or waveform averaging in post-processing. The VQ-820-G and VQ-880-G only support conditional waveform recording with sample blocks of a few meters length.

Starting with the VQ-840-G, the possibility of *unconditional* waveform recording was introduced. This means that waveforms are stored in a predefined section of the range gate for every laser shot without employing any target detection. Thus, echoes that might not have triggered OWP or waveform recording in the first place, might be recovered by further analysis in post-processing. This capability has also been enabled for the VQ-880-G II through firmware upgrade in 2022.

Online waveform processing is performed by comparing the echo signal identified by signal detection with the generic echo signal expected from an extended, flat target larger than the laser footprint, i.e. the system response (Pfennigbauer and Ullrich, 2010). This system response is determined during the instrument's calibration process and stored in the instrument. The echo signal's amplitude and range are obtained in a single optimization process which also delivers the residual, provided as pulse shape deviation attribute assigned to every target (Pfennigbauer et al., 2014).

3. STUDY AREA AND DATA SETS

The study area is an approximately 6.5 km long section of the Pieach River near Loosdorf (Lower Austria). The Pielach is a pre-alpine gravel bed river with pluvio-nival discharge regime, i.e., the annual flood peaks occur in spring during snow melt and in summer after heavy precipitation events. The Pielach is a right hand tributary of the Danube River with a mean discharge of 7 m^3/s and a mean slope of 3 ‰ within the study reach.

The river section features a near-natural character with a meandering river course, abundant deadwood in the river bed and alluvial forests to both sides of the river, which especially applies to the two designated Natura2000 nature reserve areas Ofenloch and Neubacher Au (cf. Figure 3). This enables changes of the river's gravel bed after discharge peaks and makes the study area ideal for morphodynamic monitoring (Mandlburger et al., 2015). Besides the river course, a dozen freshwater ponds are located in the surrounding flood plain. They are the result of former open pit mining activities and are now used for fishing and recreation. Depending on their use, individual ponds have varying levels of turbidity and some ponds feature submerged macrophytes, which opens up additional opportunities for bathymetric research beyond simply mapping the underwater topography.

The area was repeatedly captured since 2013 with the topo-bathymetric laser scanners described in Section 2 with at least one data acquisition per year. While we focus on acquisitions from crewed aircraft based on the VQ-820-G and VQ-880-G(II)

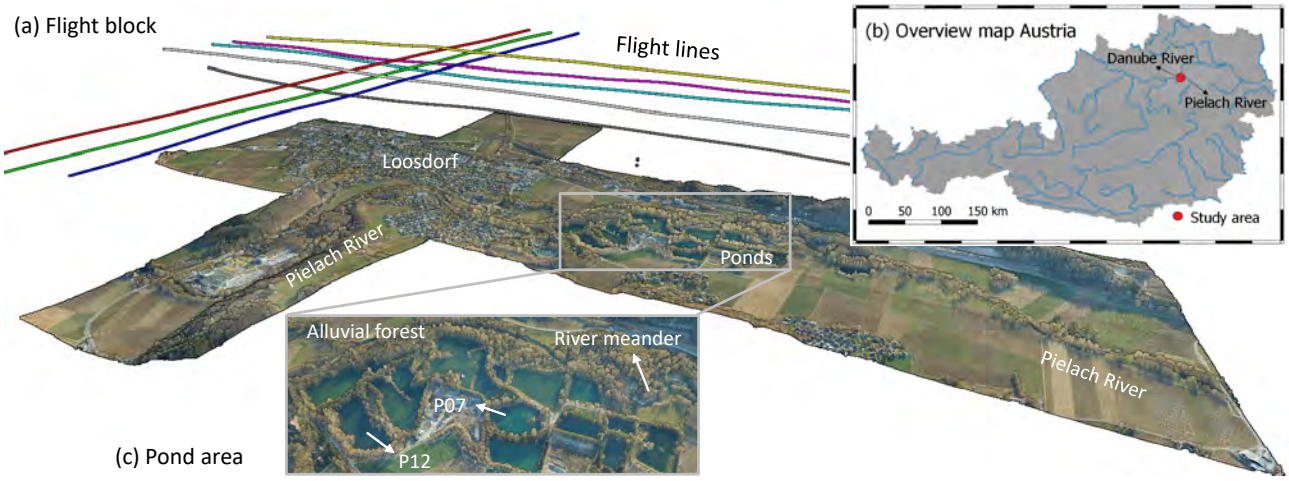

Figure 3. Study area Loosdorf/Pielach: (a) Perspective view of flight lines and colorized 3D laser point cloud acquired on Feb, 08, 2023; (b) Location of study area within Austria; (c) close-up of ponds and river meander area.

sensors in this paper, the VQ-840-G can be installed on UAV platforms allowing dm-level spatial resolution (Mandlburger et al., 2020). The best season for data capture is the leaf-off period between November and March, which also temporally correlates with low discharge periods (cf. Table 2) and, in consequence, clear water conditions. This applies to both the river course and the still freshwater ponds. From the overall pool of 25 acquisitions, we chose four representative leaf-off datasets with clear water conditions due to low precipitation and low temperatures for the comparisons in this paper. Table 2 summarizes the main flight mission parameters.

date	2014-02-21	2015-03-20	2020-03-09	2023-02-08
sensor	VQ-820-G	VQ-880-G	VQ-880-G	VQ-880-G II
flying alt. [m]	700	700	700	600/700
IR channel	no	no	yes	yes
full waveform	OWP only	OWP only	conditional	unconditional
discharge [m^3/s]	3.35	7.16	5.33	5.76
precipit. [mm]	0	0	7	0
temperat. [°C]	5.5	7.5	7.5	-1

Table 2. Flight mission parameters

4. PROCESSING METHODS

4.1 Georeferencing

Based on related work (Glira et al., 2019) and inspired by the idea of simultaneously processing all observations of the multi-sensor laser scanning system (Brun et al., 2022), (Pöppl et al., 2023) presented a new GNSS/INS/LiDAR-integration approach based on batch least-squares estimation. The method loosely couples GNSS and tightly couples INS and LiDAR measurements. The integrated adjustment allows for error modeling at the sensor level and thus reduces the risk of block deformation even without ground control, while allowing for very fine-grained trajectory correction.

The main steps of the approach are: First an initial trajectory is calculated from GNSS/INS data via batch least-squares adjustment using a Kalman filter to initialize trajectory parameters for the non-linear optimization. Secondly, the LiDAR measurements (range, scan angle) are directly georeferenced based on the initial trajectory and calibration parameters. This results in a preliminary 3D point cloud for identifying correspondences. Next, estimates of the trajectory and system calibration are optimized within a batch least-squares adjustment of all available data including GNSS, INS and LiDAR. And finally, the LiDAR data are combined with the improved trajectory and system calibration to obtain the final point cloud.

For applying this method to the Pielach River ALB data set, we extended the approach for sensors integrated into a gyro-stabilized mounting system. This was necessary for the flight mission in February 2023 (cf. Section 3 and Figure 3).

4.2 Full waveform analysis

One of the interesting features of the SVB (Schwarz et al., 2019) is the ability to enhance depth penetration with respect to plain OWP (Pfennigbauer et al., 2014). Since the underlying Exponential Decomposition (XDC) evaluates to a single coherent model of the water column, the position of the bottom is found with a higher probability than if searched with an independent trigger condition such as in the OWP case. The same also holds for the water surface.

Another, independent, approach to enhancing depth penetration is to make use of a method known as coherent integration or pre-detection integration (Skolnik, 1981), which reduces the incoherently occurring noise component by coherent superposition of repeated measurements. This leads to an improvement of the signal to noise ratio (SNR). When used with laser scanning, the method is known by the name waveform-stacking (Stilla et al., 2007). Because laser scanners usually have a different beam direction for each shot, coherence must be carefully checked or established.

The post processing software available with *RIEGL* scanners makes use of the known flight state of the platform to align the laser beams prior to averaging. The employed algorithms either perform a strict search for geometrically close neighboring laser rays or make use of the inherent neighborhood from the regular scan pattern. Averaged waveforms are computed in a rolling manner, so that the resulting point density stays the same as for the raw waveforms, which is a desired property.

Due to recent developments, both SVB and averaging, can now also be combined to obtain a cumulative effect for enhancing penetration depth.

Figure 4. Strip height differences [m] after standard strip adjustment with RiPRECISION (left) and GNSS/INS/LiDAR-integrated adjustment (right). Overlayed on the strip differences are normal distances to ground truth targets of two types: check points on horizontal surfaces on the ground (circles) and on sloped rooftops (squares), after application of the estimated datum shifts.

5. RESULTS AND DISCUSSIONS

In this section, we present the results for the four selected Pielach River datasets (2014-2023) described in Section 3 and compare existing point clouds (2014-2020) and new results obtained by applying the latest methods presented in Section 4 to the 2023 flight block.

First, we applied the extended GNSS/INS/LiDAR-integration approach detailed in Section 4.1 to the most recent data set as of February 8, 2023. Figure 4 shows the strip height differences for the integrated method (right) in comparison to a conventional strip adjustment implemented in the RiPRECISION software (left). The adjustment itself as well as the strip differences are based on both IR and green laser channels. Note that no ground control information is introduced in either version, which is less of a problem for the integrated method as comprehensive error modeling for all sensor observations reduces the risk of systematic block deformations when trying to minimize strip-to-strip deviations.

Figure 4 also shows discrepancies compared to two types of ground truth (i.e. reference) information, namely (i) 54 check points on horizontal ground surfaces and (ii) 46 check points on sloped rooftops. The discrepancies are computed as perpendicular distances from the check point to a robust best fitting planar surface of all LiDAR points (both channels) within a 1 m radius. Check points with less than 20 LiDAR points were discarded. The RMSE of point cloud w.r.t. reference surfaces is 7.5 cm for the conventional strip adjustment and 4.7 cm for the GNSS/INS/LiDAR-integrated adjustment. In this case, the data was used as-is, i.e., a true direct georeferencing. When using the point-to-surface distances to estimate and apply a datum shift (dx/dy/dz: [3.1, -5.1, 6.8] cm and [0.9, 7.4, 0.3] cm respectively), the RMSE reduces to 4 cm for both approaches.

However, in the GNSS/INS/LiDAR-integrated adjustment, the strip differences are reduced to less than 4 cm, which is a significant reduction compared to the 10 cm errors visible in the results of the standard strip adjustment. This means, that the GNSS/INS/LiDAR-integrated adjustment is able to correct trajectory errors to a much higher degree while avoiding block-deformation, due to tighter coupling between LiDAR and IMU. Thus, the internal consistency of the point cloud is improved. The remaining discrepancies are largely caused by a mismatch between the green and red channel. While this may be partially due to small remaining errors in the internal orientation of the scanners, another explanation is the differing beam characteristics of the green and red channels. Due to different beam footprints as well as pulse lengths, objects, especially if sloped, will appear at slightly different ranges. In future work, we will try to improve this by modeling such complex target situations.

To answer the question of whether pure sensor development over the past decade has effectively increased penetration depth, Figure 5 compares the results of standard online waveform processing of the four data sets from 2014, 2015, 2020, and 2023, respectively. The top row (Figure 5a-d) shows the color coded water depth maps for pond P07 depicted in Figure 3c including depth contours every 50 cm. The VQ-820-G dataset of 2014 shows void areas in the middle of the pond, where bottom points are entirely missing. The voids can be explained as this instrument only features a depth performance of 1 SD. All other datasets were acquired with VQ-880-G or G II instruments, respectively and show full coverage. However, only the 2023 dataset truly provides complete pond penetration and continuous bottom point coverage to the maximum pond depth of 4.5 m, whereas in the 2015 and 2020 datasets some points on the canopy of submerged macrophytes are classified as ground points due to the lack of vegetation penetration. The effect is more pronounced for the earlier 2015 dataset compared to the acquisition of 2020.

The depth distribution histograms (2^{nd} row of Figure 5a-d) also confirm this interpretation, with only the histogram for the year 2023 showing a pronounced tail in depths larger than 4 m, which correspond to the dark blue areas of the depth map. This tail is absent in all other datasets. Note also that the mean depth gradually increases from 2014-2023. This can also be seen from the cross section plot in Figure 5e, where the 3D point cloud of a selected profile is displayed for all four datasets. Only the violet points corresponding to the 2023 dataset show full penetration, while the yellow (2015) and orange (2020) points do not penetrate the underwater vegetation layer. Because we carefully selected data sets, all from winter seasons with comparable water conditions, we can conclude that sensor development over the past decade has resulted in a substantial increase in penetration depth.

Apart from pure sensor development, Figures 6 and 7 also demonstrate benefits resulting from improved processing algorithms exemplified for a section of the Pielach River. While the OWP points (Figure 6) are spread over the entire depth, the XCD/SVP points (Figure 7) concentrate at the surface and the bottom due

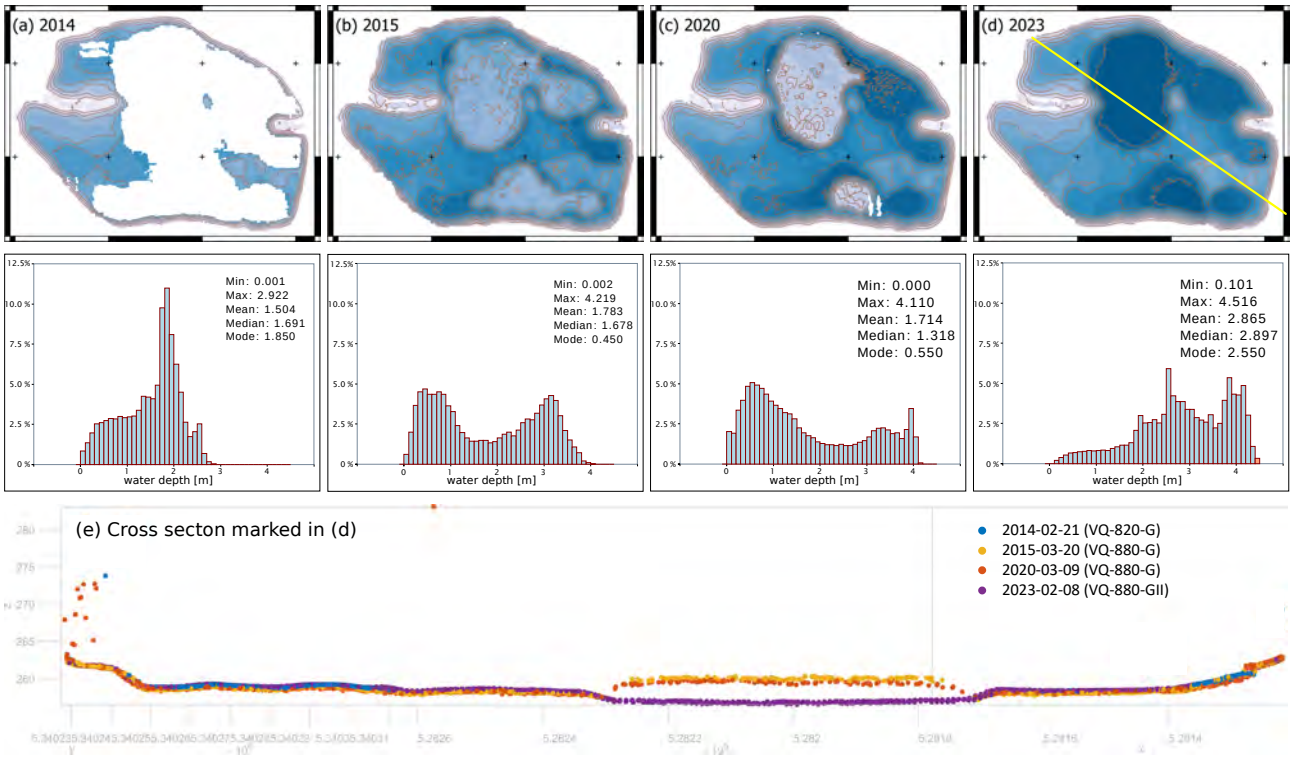

Figure 5. Multi-temporal comparison of depth penetration at pond P07 based on Online Waveform Processing; color water depth map (a) Feb 2014; (b) Mar 2015; (c) Mar 2020; (d) Feb 2023; (e) cross sectional comparison 2014-2023.

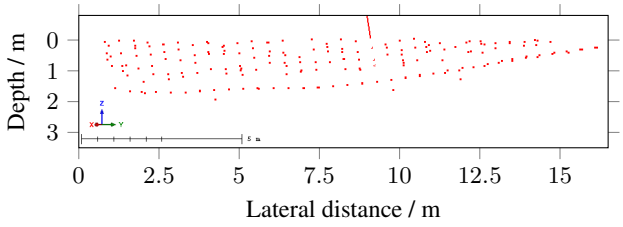

Figure 6. Profile of Pielach, online processed (OWP). Points spread over almost the whole depth.

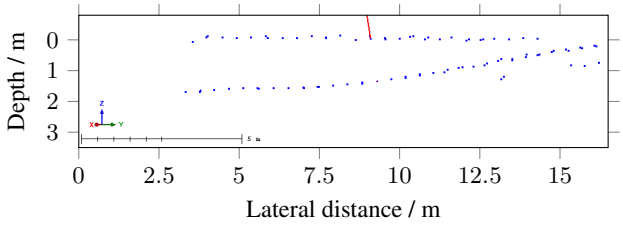

Figure 7. Profile of Pielach, exponentially decomposed (XDC, SVB). Points concentrated at the surface and bottom.

to the underlying physical model of laser light interaction with the medium water. The corresponding waveform for a selected point in Figure 7 is displayed in Figure 8 including the convolved model (black) and the exponential model (red).

Besides the much clearer point cloud, this also has a positive effect for estimating the water surface level from green laser channels. While it is known from literature (Guenther et al., 2000) that laser echos reflected from the air-water-interface show a bias due to signal components from volume backscattering in the water column, this can effectively be mitigated using the

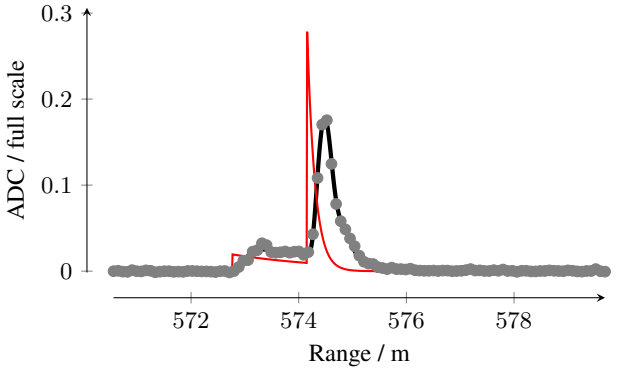

Figure 8. Full wave of Figure 7. Dots: measured points; Black line: convolved model; Red line: exponential model.

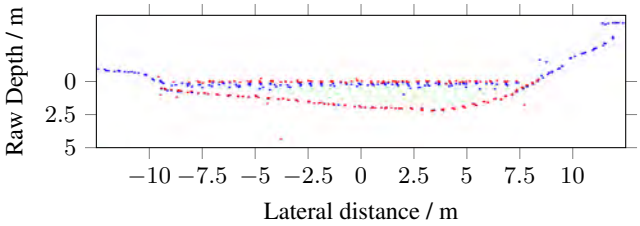

Figure 9. Algorithms comparison: Green: OWP with static trigger; Blue: SRF with dynamic trigger; Red: XDC with SVB specialisation.

SVB approach. This becomes even more apparent in Figure 9

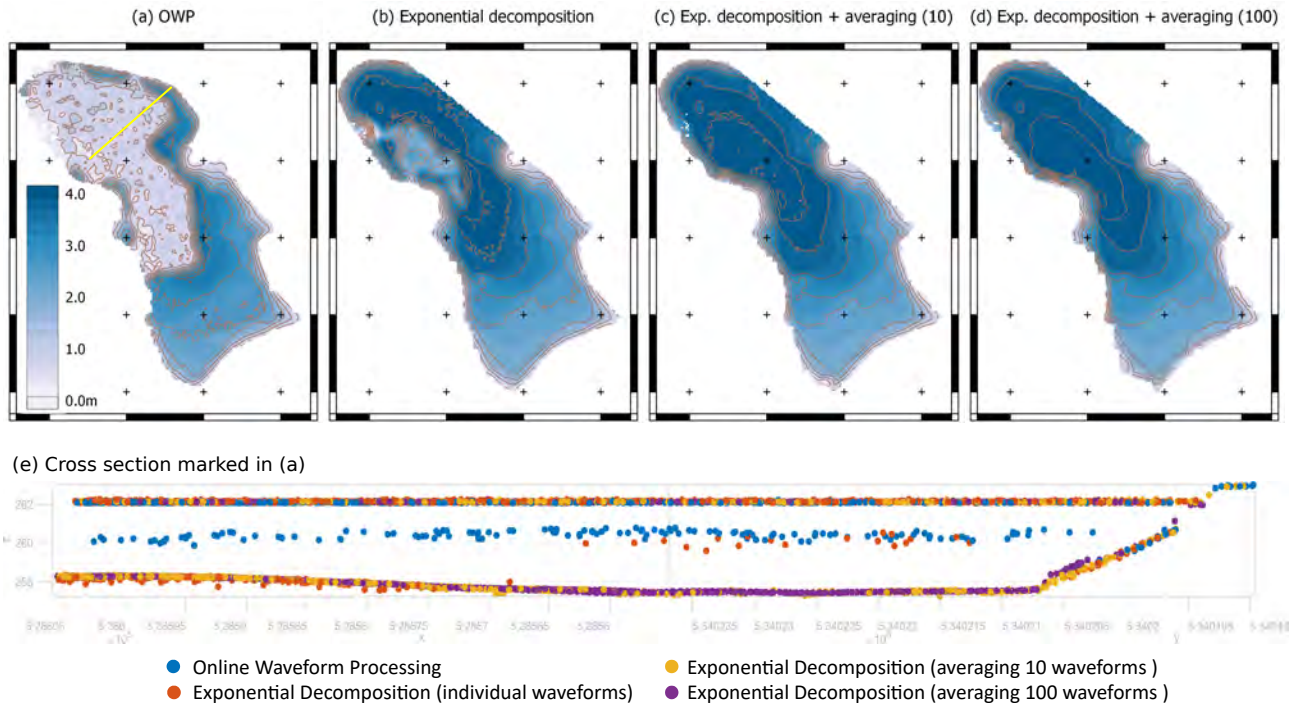

Figure 10. Depth penetration comparison using different full waveform processing strategies; (a) Online Waveform Processing (OWP); (b) Exponential Decomposition (XDC) without waveform averaging; (c) and (d) XDC with 10/100 waveforms averaged; (e) cross sectional comparison.

where OWP points (green) or SRF[2] points (blue), respectively, are overlayed with SVB points (red). The latter are higher and can therefore better compensate for near-surface penetration.

However, when it comes to the ultra shallow area with water depths less than the pulse length (i.e. approx. 25 cm), one can still see that no SVB surface echoes are resolvable in this area. While the SVB method is theoretically capable of resolving zero depths (Schwarz et al., 2019), run-time requirements of the software implementation currently impose practical limitations. In the future, we plan to use deep learning methods to anticipate challenging target situations such as very shallow areas, laser beams with complex underwater targets including submerged macrophytes or dead wood, etc.

In a final analysis, we investigate the impact of different full waveform processing methods (OWP and XDC) additionally taking into account waveform averaging on depth penetration. Figure 10 shows the results for pond P12. The pond has the same depth as P07 (4.5 m) but more turbid water conditions. The first row of Figure 10 shows from (a) to (d) color coded water depth maps superimposed with 0.5 m depth contours. In all cases, the depth maps are derived from all points classified as water bottom. All shown examples are derived from the same data basis, a flight strip captured from 600 m agl with a pulse repetition rate of 200 kHz. These settings allow storage of unconditional waveforms as described in Section 2.2.

Figure 10a shows the depth map for the standard OWP. The map shows a shallow zone in the northeastern part of the pond with depths around 1.5 m while in reality the pond exhibits its maximum depth of 4.5 m in this area. In contrast to P07 and Figure 5, where impenetrable underwater vegetation was the reason for too shallow depths, in this case it is a pure lack of depth penetration due to turbid water conditions. As a consequence, the OWP points classified as water bottom jump from the maximum OWP depth penetration of around 3 m back to a depth of approximately 1.5-2 m. These points do neither represent water bottom nor underwater vegetation canopy, but just mark the lowest detected OWP echoes (erroneously classified as bottom). This can also be clearly seen from the cross sectional view in Figure 10e, where the OWP points plotted in blue tend to ”float” at a more or less constant depth between surface and bottom.

The situation is remarkably improved when employing XDC based on the unconditional waveforms. The water depths plotted in Figure 10b show a consistent decrease from the shore down to a depth of 4 m and only the parts deeper than 4 m are not penetrable for XCD performed on single waveforms. Correspondingly, most of the yellow points in Figure 10 align to the pond’s bottom and only a few points float somewhere between surface and bottom.

Exponential decomposition of a waveform averaged from ten surrounding laser shots further improves depth measurement performance (cf. Figure 10c and orange points in Figure 10e). With this variant, full penetration of the pond can be achieved but the bottom point density drops sharply at a depth of approximately 4.2 m. Only when 100 waveforms are averaged, full penetration is reached with full point density (violet points in Figure 10e). However, averaging at such a high level substantially decreases the spatial resolution resulting in overly smoothed depth contour lines (cf. Figure 10d). Thus, waveform averaging should only be used if XCD performed on individual waveforms fails to entirely penetrate the water body. Such a pivot based approach is also suggested by other authors in the field (Mader et al., 2022).

[2] SRF = System Response Fitting = off-line version of OWP

6. CONCLUSIONS

In this article, we have highlighted the advancements in topo-bathymetric laser scanning over the past decade in terms of sensors and algorithms. Advances in georeferencing ALB data using an integrated approach where GNSS, INS, and LiDAR measurements are processed simultaneously have proven to be a significant step towards true direct georeferencing without additional control information. This if of specific importance for long-term monitoring of water bodies as, for instance, requested by the Water Framework Directive of the European Union.

We were also able to show that for the acquisition of 3D dense underwater point clouds with sub-meter spatial resolution, sensor improvements alone resulted in an increase of the achievable penetration depth to more than 2 times Secchi depth. In addition, customized evaluation algorithms are also available today, which on the one hand allow greater penetration depths, but on the other hand also improve detection and modeling of the dynamic water surface. The latter is a precondition for precise refraction correction and thus further reduces the Total Vertical Uncertainty of the bathymetry.

In future work, we will incorporate machine learning to identify complex target situations and thereby better address specific situations such as very shallow areas or locations with vegetation above and below the water surface. For the mentioned research questions, the meanwhile 10 years of measurements on the Pielach River represent a valuable data base.

REFERENCES

Brun, A., Cucci, D. A., Skaloud, J., 2022. LiDAR Point–to–Point Correspondences for Rigorous Registration of Kinematic Scanning in Dynamic Networks. *ISPRS Journal of Photogrammetry and Remote Sensing*, 189, 185–200.

Cucci, D. A., Rehak, M., Skaloud, J., 2017. Bundle Adjustment with Raw Inertial Observations in UAV Applications. *ISPRS Journal of Photogrammetry and Remote Sensing*, 130, 1–12.

Effler, S. W., 1988. Secchi Disc Transparency and Turbidity. *Journal of Environmental Engineering*, 114(6), 1436-1447. https://ascelibrary.org/doi/abs/10.1061/%28ASCE%290733-9372%281988%29114%3A6%281436%29.

Eren, F., Jung, J., Parrish, C. E., Sarkozi-Forfinski, N., Calder, B. R., 2019. Total Vertical Uncertainty (TVU) Modeling for Topo-Bathymetric LIDAR Systems. *Photogrammetric Engineering and Remote Sensing*, 85(8), 585–596.

Glira, P., Pfeifer, N., Mandlburger, G., 2019. HYBRID ORIENTATION of AIRBORNE LIDAR POINT CLOUDS and AERIAL IMAGES. *ISPRS Annals of the Photogrammetry, Remote Sensing and Spatial Information Sciences*, 4number 2/W5.

Gordon, H. R., Brown, O. B., Jacobs, M. M., 1975. Computed Relationships Between the Inherent and Apparent Optical Properties of a Flat Homogeneous Ocean. *Appl. Opt.*, 14(2), 417–427. https://opg.optica.org/ao/abstract.cfm?URI=ao-14-2-417.

Guenther, G. C., Goodman, L. R., 1978. Laser Applications For Near-Shore Nautical Charting. M. B. White, R. Stevenson (eds), *Ocean Optics V*, 0160, International Society for Optics and Photonics, SPIE, 174–183.

Guenther, G., Cunningham, A., Laroque, P., Reid, D., 2000. Meeting the accuracy challenge in airborne lidar bathymetry. *Proceedings of the 20th EARSeL Symposium: Workshop on Lidar Remote Sensing of Land and Sea*, Dresden, Germany.

Hansen, S. S., Ernstsen, V. B., Andersen, M. S., Al-Hamdani, Z., Baran, R., Niederwieser, M., Steinbacher, F., Kroon, A., 2021. Classification of Boulders in Coastal Environments Using Random Forest Machine Learning on Topo-Bathymetric LiDAR Data. *Remote Sensing*, 13(20). https://www.mdpi.com/2072-4292/13/20/4101.

IHO, 2020. S-44, Standards for Hydrographic Surveys, Edition 6.0. Standard 5th ed., International Hydrographic Organization, Monaco.

Kinzel, P. J., Legleiter, C. J., Nelson, J. M., 2013. Mapping River Bathymetry With a Small Footprint Green LiDAR: Applications and Challenges. *JAWRA Journal of the American Water Resources Association*, 49(1), 183–204. http://dx.doi.org/10.1111/jawr.12008.

Mader, D., Richter, K., Westfeld, P., Maas, H.-G., 2022. Potential of a Non-linear Full-Waveform Stacking Technique in Airborne LiDAR Bathymetry, journal=PFG – Journal of Photogrammetry, Remote Sensing and Geoinformation Science. https://doi.org/10.1007/s41064-022-00212-0.

Mandlburger, G., Hauer, C., Wieser, M., Pfeifer, N., 2015. Topo-bathymetric LiDAR for monitoring river morphodynamics and instream habitats-A case study at the Pielach River. *Remote Sensing*, 7(5), 6160–6195. http://www.mdpi.com/2072-4292/7/5/6160.

Mandlburger, G., Pfennigbauer, M., Schwarz, R., Flöry, S., Nussbaumer, L., 2020. Concept and Performance Evaluation of a Novel UAV-Borne Topo-Bathymetric LiDAR Sensor. *Remote Sensing*, 12(6), 986. https://www.mdpi.com/2072-4292/12/6/986.

Pfennigbauer, M., Ullrich, A., 2010. Improving quality of laser scanning data acquisition through calibrated amplitude and pulse deviation measurement. *Proc.SPIE*, 7684, 7684 – 7684 – 53.

Pfennigbauer, M., Wolf, C., Weinkopf, J., Ullrich, A., 2014. Online waveform processing for demanding target situations. *Proc. SPIE*, 90800J.

Philpot, W. (ed.), 2019. *Airborne Laser Hydrography II*. Cornell University Library (eCommons), Coernell.

Pöppl, F., Pfennigbauer, M., Ullrich, A., Mandlburger, G., Neuner, H., Pfeifer, N., 2023. Modelling of GNSS Positioning Errors in a GNSS/INS/LiDAR-integrated Georeferencing. *Publikationen der Deutschen Gesellschaft für Photogrammetrie, Fernerkundung und Geoinformation e.V.*, 183–196.

Quadros, N. D., 2013. Unlocking the characteristics of bathymetric LiDAR sensors.

Schwarz, R., Mandlburger, G., Pfennigbauer, M., Pfeifer, N., 2019. Design and evaluation of a full-wave surface and bottom-detection algorithm for LiDAR bathymetry of very shallow waters. *ISPRS Journal of Photogrammetry and Remote Sensing*, 150.

Schwarz, R., Pfeifer, N., Pfennigbauer, M., Ullrich, A., 2017. Exponential Decomposition with Implicit Deconvolution of Lidar Backscatter from the Water Column. *PFG – Journal of Photogrammetry, Remote Sensing and Geoinformation Science*, 85(3), 159–167. https://doi.org/10.1007/s41064-017-0018-z.

Skolnik, M. I., 1981. *Introduction to radar systems*. 2 edn, McGraw-Hill Book Co. bibtex: skolnik_introduction_1981.

Stilla, U., Yao, W., Jutzi, B., 2007. Detection of Weak Laser Pulses by Full Waveform Stacking.

Wang, D., Xing, S., He, Y., Yu, J., Xu, Q., Li, P., 2022. Evaluation of a New Lightweight UAV-Borne Topo-Bathymetric LiDAR for Shallow Water Bathymetry and Object Detection. *Sensors*, 22(4). https://www.mdpi.com/1424-8220/22/4/1379.

Xing, S., Wang, D., Xu, Q., Lin, Y., Li, P., Jiao, L., Zhang, X., Liu, C., 2019. A Depth-Adaptive Waveform Decomposition Method for Airborne LiDAR Bathymetry. *Sensors*, 19(23). https://www.mdpi.com/1424-8220/19/23/5065.